

The thermal boundary layer effects on line-of-sight TDLAS gas concentration measurements

Zhechao Qu, Olav Werhahn, Volker Ebert

Physikalisch-Technische Bundesanstalt, Bundesallee 100, D-38116 Braunschweig, Germany

Abstract

The effects of thermal boundary layers on TDLAS measurement results must be quantified when using the line-of-sight (LOS) tunable diode laser absorption spectroscopy (TDLAS) under conditions with temperature gradients. In this paper, a new methodology based on spectral simulation is presented quantifying the LOS TDLAS measurement deviation under conditions with thermal boundary layers. The effects of different temperature gradients and thermal boundary layer thickness on spectral collisional widths and gas concentration measurements are quantified. A CO₂ TDLAS spectrometer, which has two gas cells to generate the temperature gradients, was employed to validate the simulation results. The measured deviations and collisional widths are in very good agreement with the simulated results for conditions with different temperature gradients. We demonstrate the quantification of the thermal boundary layers thickness with the proposed method by extracting collisional width from the path-integrated spectrum.

Key words

TDLAS, boundary layer, temperature gradient, gas concentration, line-of-sight

Introduction

Tunable diode laser absorption spectroscopy (TDLAS) is frequently used in science and industry for online and in situ gas analysis and has become a proven method of gas diagnostics.¹⁻⁵ Online in situ open-path TDLAS instruments do not require to take a gas sample into a closed measurement cell. This has the advantage of circumventing typical sampling problems like chemical reactions in the sampling line, delay and integration effects due to the gas transport, or wall adsorption in the sampling pipes. Absolute chemical species measurements using calibration-free TDLAS techniques need accurate measurements of the physicochemical boundary layers' conditions,¹ e.g. parameters like gas temperature and pressure. This TDLAS is one of the line-of-sight (LOS) absorption spectroscopy techniques, and its application is normally limited to flow fields with constant or negligible temperature gradients. In most single wavelength LOS TDLAS applications, uniform conditions are assumed. This constitutes a drawback in many applications, for example, when large and unexpected temperature and/or concentration gradients along the LOS may occur. The effect of boundary layers on experimental data must be well understood for a successful diagnostic measurement using LOS absorption spectroscopy.⁶⁻⁹

A lot of research efforts have been invested in absorption spectroscopy strategies for minimizing the effects of boundary layers on the LOS TDLAS measurements^{6, 10-19} or recovering spatial distribution by using tomographic inversion techniques.²⁰⁻²⁴ In combustion environments, less temperature dependent lines were used under conditions with temperature gradients to minimize the thermal boundary layers effects on gas concentration

measurements,¹¹⁻¹² and both transitions and modulation depths were carefully selected to minimize the variation and gradients in pressure and absorber concentration to achieve an accurate gas temperature measurement in the gasifier reactor core based on two-line thermometry.¹⁴ A strategy of wavelength-modulation spectroscopy (WMS) based TDLAS was developed immune to the errors of two-line thermometry measurements caused by the LOS gradients in temperature, pressure, and concentration by using two absorption transitions with strengths that scale linearly with temperature over the domain of the temperature gradient.¹⁶ The error caused by temperature and velocity gradients along the LOS in velocity measurement using WMS-TDLAS was analysed.¹⁷⁻¹⁸ But there has been a lack of quantitative analysis on the effect of temperature gradients across the LOS laser spectroscopy for gas concentration measurements.

An alternative and more complicated strategy that can significantly improve on the LOS TDLAS under non-uniform conditions is the combination of tomographic absorption spectroscopy (TAS).²⁰ The TAS solution for spatially resolved non-uniform fields from the LOS data, multiple measurement paths²⁴/wavelengths²¹⁻²³ have to be combined into a tomographic setup, the temperature or concentration gradients can be retrieved by making the use of nonlinear and linear regularization methods. It is obvious that the TAS makes both instrument and data analysis more complicated and costly than the single wavelength TDLAS. In non-uniform conditions, the path integrated spectrum of direct TDLAS (dTDLAS) is different from the simulation performed with path averaged conditions along the LOS. The errors of concentration measurements can be deduced by comparing the integrated absorption coefficient⁶ or the peak absorbance¹⁶ from the path integrated spectrum and that of the simulation performed with the path averaged uniform condition. But the path-averaged information, e.g. temperature, is not always available in many applications such as cross stack emission monitoring. Using the optical transfer standard-dTDLAS method under conditions with temperature and/or concentration gradients,²⁵⁻²⁶ the path-integrated spectra are measured together with temperature and pressure measurements (one or several sampling points along the LOS). The question is how to evaluate the measured spectra under such conditions. The derived concentration is different when using path-averaged, wall or core temperature/pressure to evaluate the spectra. It is essential to know the deviation of the deduced concentration from the measured path integrated spectrum when a LOS gradient is present.

In this work, we present a methodology for quantifying the deviation of dTDLAS concentration measurements under the conditions with thermal boundary layers. The use of two-cell based dTDLAS CO₂ spectrometer enabled a validation of the simulated results. It is shown that the simulated results had very good agreement with the measurements. The method was also applied to estimate the thermal boundary layer's thickness from the collisional widths of path-integrated spectra and to investigate temperature gradient effects.

Theory

Tunable diode laser absorption spectroscopy

In TDLAS, the wavelength λ of a tunable laser is rapidly scanned across a narrow region of the optical spectrum covering one or several electronic, vibrational or rotational-vibrational absorption lines. The intensity of the laser light, $I(\lambda)$, focused onto a photodetector after passing the sample with absorbers can be described by the extended Lambert-Beer law according to

$$I(\lambda) = E(t) + I_0(\lambda) \cdot T(t) \cdot \exp[-S(T) \cdot g(\lambda - \lambda_0) \cdot n \cdot L], \quad (1)$$

with the background emission $E(t)$ at time t , initial laser intensity $I_0(\lambda)$, and the broadband transmission losses $T(t)$ which are synchronously derived from the individual raw signals and absorption profiles. The exponential term embraces the absorption line strength $S(T)$ at gas

temperature T , the normalised (area=1) line shape function $g(\lambda-\lambda_0)$ (centred at the wavelength λ_0), the absorber number density n and the optical path length L .

By combining Eq. 1 and the ideal gas law, the gas concentration (amount fraction) x is

$$x = \frac{k_B \cdot T}{S(T) \cdot r_{iso} \cdot L \cdot p_{total}} \int \ln\left(\frac{I(\lambda) - E(t)}{I_0(\lambda) \cdot Tr(t)}\right) \frac{d\lambda}{dt} dt = \frac{k_B \cdot T \cdot A_{line}}{S(T) \cdot r_{iso} \cdot L \cdot p_{total}}, \quad (2)$$

where k_B is the Boltzmann constant, p_{total} is the total pressure of the gas sample, r_{iso} is a correction factor for the isotopic composition in the gas sample, and A_{line} is the line area determined by spectral integration of the measured absorption line over the wavenumber axis. $d\lambda/dt$ describes the dynamic wavelength tuning coefficient of the laser, which has to be determined experimentally. This is extracted from the Airy-signal when the laser light is transmitted through an optical etalon.

The Voigt function was used to model the lineshape of the transition, which considers the combined effects of Doppler and collisional broadening on the spectrum. These effects are characterized by the Doppler broadening full width at half maximum (FWHM), $\Delta\nu_D$ (cm^{-1}), and the collisional-broadening FWHM, $\Delta\nu_L$ (cm^{-1}), given by

$$\Delta\nu_D = \nu_0 \sqrt{\frac{8k_B T \ln 2}{Mc^2}}, \quad (3)$$

$$\Delta\nu_L = 2\gamma_{self} \cdot p_{self} \cdot \left(\frac{T_0}{T}\right)^{n_{self}} + 2\sum_f \gamma_f \cdot p_f \cdot \left(\frac{T_0}{T}\right)^{n_f}, \quad (4)$$

where M is the molecular mass of the absorbing species, the coefficients γ_{self} and γ_f are the self and foreign (e.g. air or N_2) broadening coefficients, p_{self} and p_f are the partial pressures of the analyte, e.g. CO_2 , and the foreign molecules, respectively, n_{self} and n_f are the temperature dependence of the collisional broadening which must be specifically considered when the temperature is far away from the reference temperature $T_0=296$ K. Typical values for n_{self} and n_f are between 0.4 and 0.9. Normally, Doppler broadening can be calculated directly using Eq. 3 and thus does not have to be fitted, if the gas temperature is measured in the experiment with sufficient accuracy. When the pressure increases to 1 bar or higher, the Doppler width becomes much smaller than the collisional width. In this condition, the Doppler width should be fixed and calculated with Eq. 3 while doing the Voigt lineshape fitting.

In temperature uniform conditions, the calculation temperature T in Eq. 2, should be known to calculate the gas concentration, and the line strength $S(T)$ according to

$$S(T) = S(T_0) \cdot \frac{Q(T_0)}{Q(T)} \cdot \exp\left[-\frac{h \cdot c \cdot E''}{k_B} \left(\frac{1}{T} - \frac{1}{T_0}\right)\right] \cdot \frac{1 - \exp[-h \cdot c \cdot \nu_0 / (k_B \cdot T)]}{1 - \exp[-h \cdot c \cdot \nu_0 / (k_B \cdot T_0)]}, \quad (5)$$

where Q is partition sum, h is the Planck constant, c is the speed of light in vacuum, E'' is the lower state energy of the transition, ν_0 is the spectral transition wavenumber, and $S(T_0)$ is the line strength given for the reference temperature ($T_0=296$ K).

It is clear that the gas concentration x , as well as $S(T)$, can be calculated using the calculation temperature T which is constant along the LOS in uniform conditions. But, it is not the case in conditions with thermal boundary layers. TDLAS measurements are path-integrated, i.e. the temperature at each point along the beam path is incorporated into the detected absorption feature. Using different calculation temperature (e.g. path-averaged, maximum or minimum temperature along the LOS) derives different concentration result. The effects of the thermal boundary layers in the test gas on the LOS absorption measurements can be addressed by simulating path-integrated spectra. This allows for boundary layer effects on concentration measurements to be quantified and enables the development of guidelines for desensitizing the LOS measurements to non-uniform fields e.g. stacks or combustion chambers.

Line temperature dependence

To estimate the relative influence of thermal boundary layers, the temperature dependence of the target transition line has to be analyzed. Figure 1a shows two forms of the temperature dependence of the CO₂ P36e transition line, one is the number density normalized temperature dependence $S(T)$ with the unit of cm⁻¹/molecules·cm⁻², the other is $S(T)/T$ with the unit of cm⁻¹/molecules·cm⁻²·K. The temperature independence positions of these two forms are 454 K and 321 K for $S(T)$ and $S(T)/T$, respectively. According to Eq. 2, if the species concentration x is to be measured, the temperature dependence of $S(T)/T$ should be analyzed, dashed curve in Figure 1a. Otherwise, number density normalized temperature dependence $S(T)$ is used when measuring the number density n . This paper focuses on the concentration measurement, so that the derivative and temperature coefficient of $S(T)/T$ are shown in Figure 1b. Around the $S(T)/T$ maximum near 321 K the temperature dependence is negligible, whereas for the further distant temperatures the influence of the temperature measurement uncertainty increases. The temperature coefficient shows the line strength $S(T)/T$ changes from -0.4 to 0.8 %/K in the full range. This is beneficial to estimate whether a transition line is good enough for certain applications, especially under conditions with varying temperature. If the gas temperature varies along the LOS, the gas concentration cannot be predicted accurately from the measured integrated area without knowledge of the temperature distribution along the LOS.

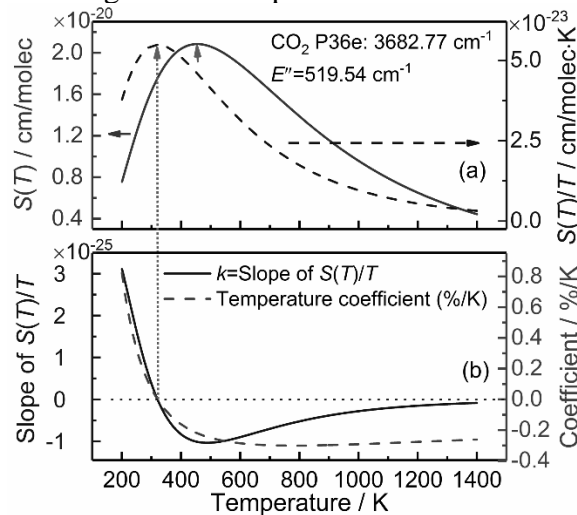


Figure 1. (a) Temperature behavior of the line strength for the CO₂ P36e transition line, the line data are from HITRAN;²⁷ solid: $S(T)$ --cm/molec; dash: $S(T)/T$ --cm/molec·K. (b) The derivative (solid) and temperature (dash) coefficient of $S(T)/T$.

Scheme of modelling thermal boundary layer effect

To quantify the deviation of concentration measurements with the LOS TDLAS technique under conditions with varying temperature, we consider a two-zone temperature distribution across the LOS as shown in Figure 2a, with low temperature zone at T_1 and L_1 , and T_2 and L_2 for the high temperature zone. To investigate the thermal boundary layer effects, the basic idea is to derive the concentration from a simulated path-integrated spectrum under such conditions. The different calculation temperature, e.g. path-averaged temperature T_{ave} , maximum temperature along LOS T_{max} , or minimum temperature along LOS T_{min} , used in Eqs. 2 and 5 skews the measurement results differently. The deviation is defined as the discrepancy between the derived concentration and the initial concentration used to simulate the path-integrated spectrum. It is a straightforward way to estimate the deviation of TDALS concentration measurements in real applications. The deviation depends on which calculation temperature is used to evaluate the measured path-integrated spectrum. The simulation routine shown in Fig. 2b was used: A) simulate the path-integrated spectrum with the input parameters (T_i , L_i , p_i and initial concentration C_i) and the transition line data, e.g. from HITRAN; B) fit the simulated

spectrum and derive the area and collisional width; C) choose the calculation temperature (T_{ave} , T_{min} or T_{max}) to derive the concentration x ; D) calculate the deviation Δx by comparing the derived concentration x and the value of C_{ave} which is used to simulate the spectrum. This strategy can be applied to the LOS TDLAS to quantify the deviation of concentration measurement under any conditions with boundary layers.

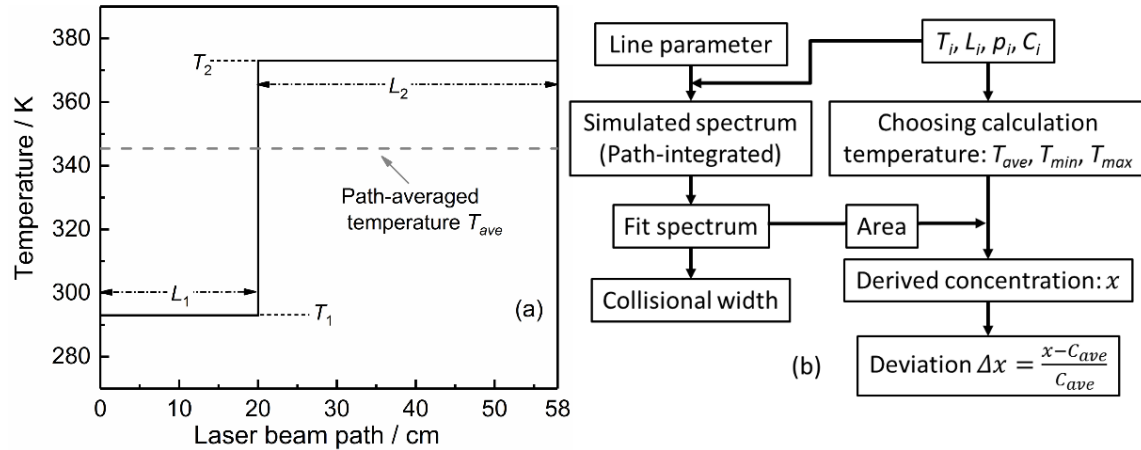


Figure 2. (a) Two-zone temperature distribution across the simulated LOS, low temperature zone with T_1 and L_1 , high temperature zone with T_2 and L_2 . (b) Flow chart of the simulation scheme to calculate the concentration deviation, T_i , L_i , p_i and C_i are the temperature, path length, pressure and initial concentration of the i -th section, $C_{ave} = \frac{\sum C_i L_i}{\sum L_i}$ (if $C_i \neq C_{i+1}$).

Deviations of concentration measurement under non-uniform conditions

The strategy of quantifying the deviation of dTDLAS concentration measurements shown in Figure 2b is demonstrated with simulated path-integrated spectra for different thermal boundary layer conditions. More generally, this strategy can be applied to any LOS gradients, not only for temperature gradients, but also for concentration gradients. Figure 3 shows the simulated deviations of concentration measurements based on different calculation temperatures (T_{ave} , T_{min} and T_{max}) under a two-zone temperature profile for the CO_2 transition line shown in Fig. 1. In this demonstration, the high T_2 and low T_1 temperatures were fixed at 393 and 293 K, respectively. The high/low temperature path length ratio (L_2/L_1) across the LOS was changed to be representative of different thermal boundary layer thickness. When using the path-averaged temperature T_{ave} as the calculation temperature in Eqs. 2 and 5, the largest deviation appeared at L_2/L_1 around 1 where thermal boundary layer is largest. Obviously, the deviation increases using calculation temperature of T_{min} (or T_{max}) when the path length ratio L_2/L_1 increases (or decreases). For example, in the scenario of stack monitoring if only wall or core temperature is measured, the maximum deviation of concentration measurement under this two-zone temperature ($T_1=293$ K, $T_2=393$ K) distribution is about 4.6 %, this value will change when varying T_1 or T_2 as we can see in the following section. Note that using T_{ave} as calculation temperature doesn't always have lowest deviation which can be seen from Fig. 3. The deviation of derived concentration does not only depend on the LOS temperature profile but also on the transition line's temperature dependence $S(T)/T$.

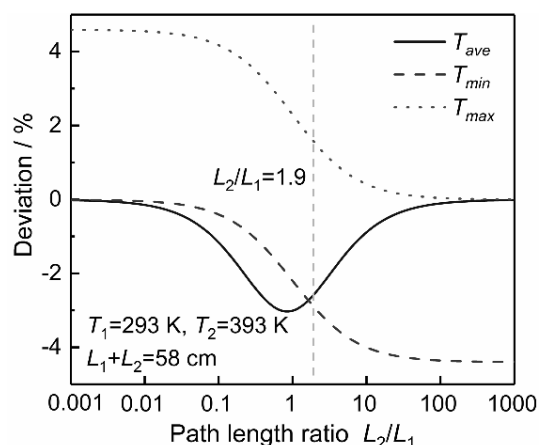


Figure 3. Simulated deviations of concentration measurements based on different calculation temperatures T_{ave} , T_{min} , and T_{max} under two-zone temperature profile as shown in Fig. 2a with different boundary layer thickness.

Figure 4 shows the simulated deviations of a fixed thermal boundary layer thickness $L_2/L_1 = 1.9$ with varying temperatures T_1 and T_2 for the P36e CO_2 transition line. Using a calculation temperature T_{ave} as shown in Fig. 4a, the deviation (underestimated) increases as T_2 is increasing when T_1 is smaller than 320 K; the deviation (overestimated) increases as T_2 increasing when T_1 larger than 450 K. Figures 4b and 4c show the results using the calculation temperature T_{min} ($=T_1$) and T_{max} ($=T_2$), respectively. The derived concentrations under conditions with temperature gradients shown in Fig. 4 are always underestimated when using T_{min} as calculation temperature, while overestimated using T_{max} . Different calculation temperature chosen for Eqs. 2 and 5 leads to different deviation. In dTDLAS applications under non-uniform conditions, the transitions line and calculation temperature should be carefully selected to minimize the deviation. In most real scenarios, the real time in situ path-averaged temperature T_{ave} is unavailable for TDLAS spectral evaluation. For example, in stack application, only the wall temperature is measured in most cases, the core temperature is rarely measured. This means only wall temperature (e.g. T_{min}) is available for TDLAS spectrometer to derive the concentration. It is essential to quantify the systematic deviation of implementing the LOS TDLAS under non-uniform conditions with the proposed method in Fig. 2b for an estimated or measured temperature gradient.

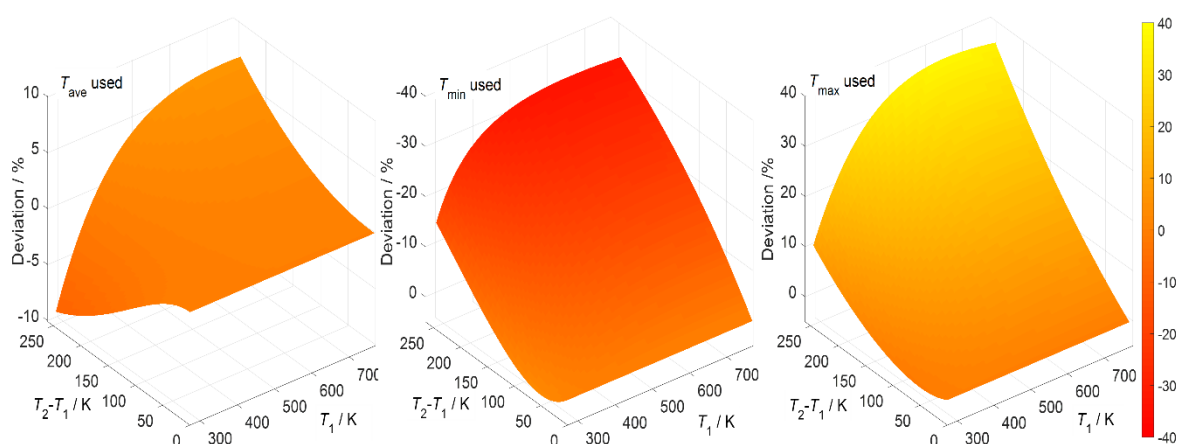


Figure 4. Simulated deviations of concentration measurements with different thermal boundary layers and calculation temperatures. T_{ave} (a), T_{min} (b) and T_{max} (c) was used in Eqs. 2 and 5 to calculate the concentration, respectively.

Thermal boundary layer effects on collisional width

According to Eqs. 3 and 4, the Doppler and collisional widths are nonlinearly dependent on temperature. As a result, if the gas temperature varies along the LOS, both widths from the line shape of path-integrated absorbance spectra will be different from uniform conditions. Figure 5a shows the collisional widths of the path-integrated spectra under corresponding conditions with temperature gradients shown in Fig. 3. Note that, the Voigt function was used to fit the path-integrated spectra with fixed Doppler width. Three almost overlapping curves in Fig. 5a are calculated based on different Doppler widths which were calculated based on Eq. 4 using different calculation temperatures (T_{ave} , T_{min} and T_{max}). Because the pressure used in the simulation was 770 mbar, the Doppler width was much smaller than the collisional width, and should be fixed while doing the Voigt fitting. Figure 5b shows the standard deviations of the residuals of Voigt fitting under each condition in Fig. 5a. The largest standard deviation was observed at the condition with the thermal boundary layer ratio L_2/L_1 around 1. The 3D plot in Fig. 5c shows the collisional widths under different temperature gradients. The collisional width monotonically changes with L_2/L_1 for fixed T_1 and T_2 . On the other hand, the thermal boundary layer thickness can be roughly estimated by the measured collisional width together with T_1 and T_2 . For example, in applications of stack or flat-flame measurements (assuming two-zone temperature profile), based on the wall T_1 and core T_2 temperatures, and measured collisional width of the path-integrated spectrum, the thermal boundary layer thickness can be estimated using this simulation method; an example will be shown in section 3. However, when the boundary layer is very thin (e.g. $L_2/L_1 < 0.1$ or $L_2/L_1 > 10$), the collisional width weakly decreases with increasing L_2/L_1 , there will be a large uncertainty in the thermal boundary layer estimation due to the collisional width is insensitive to the thermal boundary layer when approaching to **uniform** situations.

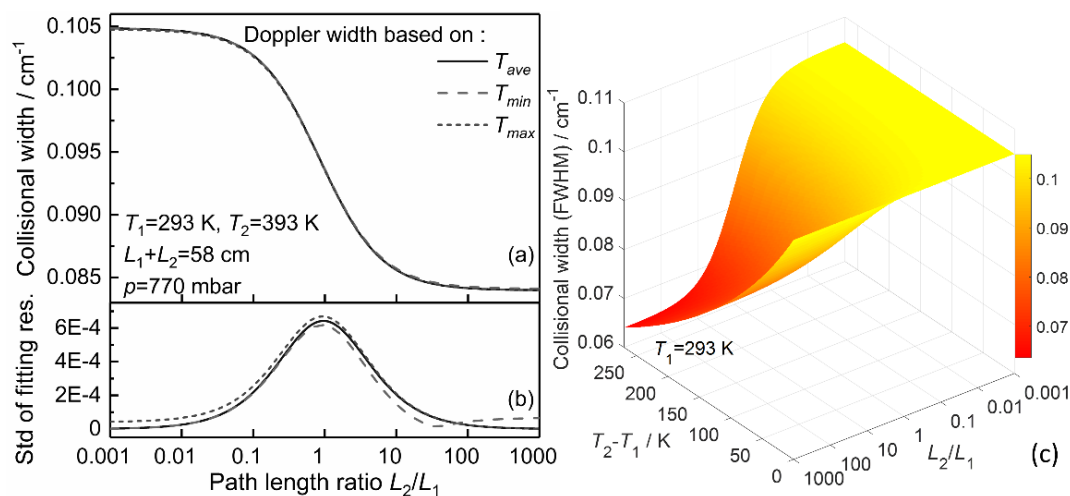


Figure 5. (a) Fitted collisional widths under different boundary layer ratio (L_2/L_1) with $L_1 + L_2 = 58$ cm, $T_1 = 293$ K, $T_2 = 393$ K, $p = 770$ mbar, three curves correspond to different Doppler width which was calculated based on different temperature (T_{ave} , T_{min} or T_{max}). (b) Standard deviations of the residuals of Voigt fitting corresponding to the conditions in (a). (c) Fitted collisional widths with varying T_2 (293 to 560 K) and L_2/L_1 (0.001 to 1000).

Validation and demonstration

Spectrometer performance

In the demonstration experiment, a two-zone temperature distribution was created in a laboratory setup using two gas cells. A schematic drawing of the experimental setup is shown in Figure 6a. A distributed feedback (DFB) diode laser at 2715 nm (Nanoplus GmbH) which has a tuning rate of 0.4 nm/K by temperature and 0.01 nm/mA by current was used to scan across the CO₂ P36e absorption line.²⁸ The laser injection current was supplied by a low-noise

driver (Thorlabs, LDC8002&TEC8020), which also controlled the diode temperature. The scan was achieved by varying the laser current with a 139.8 Hz triangular wave generated by a function generator (Agilent, 33220A). The laser beam was directed through the gas cells and then focused onto a photodetector. The detector signal was sampled at 600 kHz (National Instruments, PXIe-6124). Data acquisition and spectral fitting were controlled via LabVIEW.

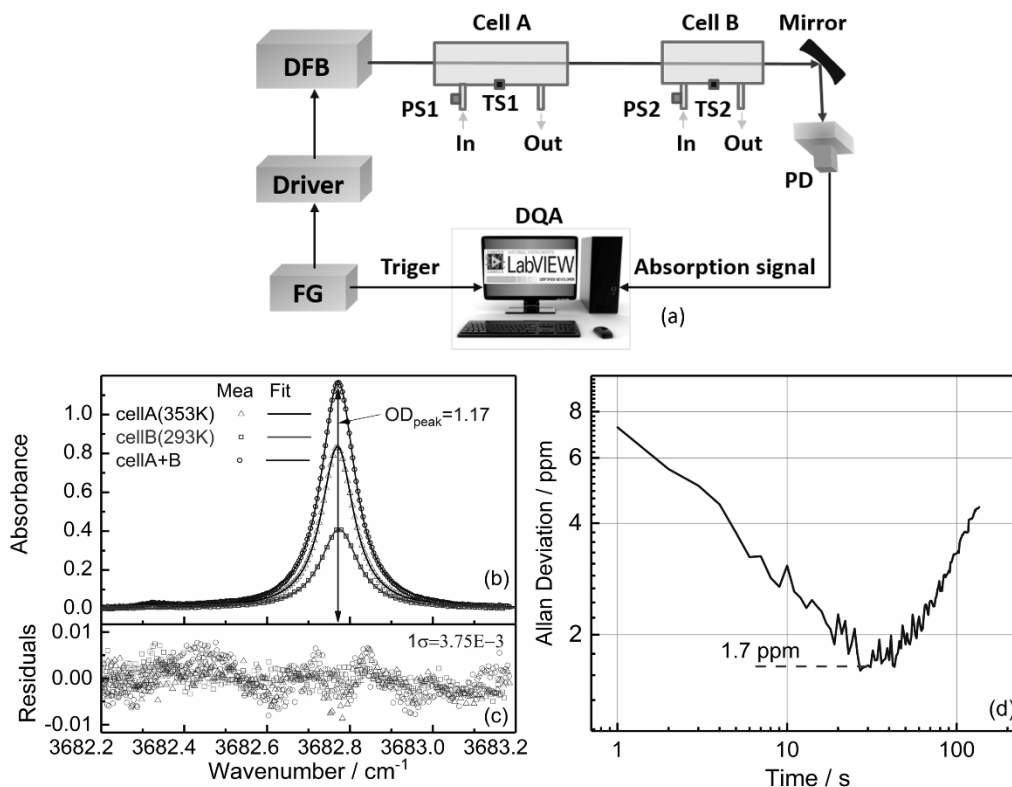


Figure 6. (a) Schematic drawing of the experimental TDLAS setup, PS-pressure sensor, TS-temperature sensor, PD-photodetector, FG-function generator, DQA-data acquisition card. (b) Measured CO₂ (P36e line, 770 mbar, 0.01 mol/mol CO₂ in N₂) spectra under different conditions; Triangle: cell A spectrum at 353 K; Square: cell B spectrum at 293 K; Circle: cell A+B spectrum under varying temperature condition. (c) The residuals of the Voigt fit to the measured data were shown in (b). (d) The Allan deviation plot of this spectrometer.

To generate the thermal boundary layers along the LOS, two cells were used along the beam path with a total optical path length of 58 cm. Cell A with 38 cm path length can be heated up to 600°C by an electronic heating system (SITEC, 772.5011-K), while cell B was used at room temperature with 20 cm length. Pressure and temperature inside both cells were continuously measured by pressure sensors and PT100 temperature sensors.

The performance of the TDLAS spectrometer was evaluated in terms of sensitivity, precision and stability. The concentration of 0.01 mol/mol CO₂ in N₂ test gas was used in the experiments. The typical measured absorption profiles with fitted Voigt profiles are shown in Fig. 6b (averaged over 10 individual scans, $\Delta t=3$ s), as well as the residuals (Fig. 6c) between the measured data and the Voigt fitting. The ‘Triangle’ absorption spectrum was measured in the condition of heating cell A to 353 K (test gas pressure in cell A was 770 mbar) and evacuating cell B. The ‘Square’ spectrum was measured at cell B filled with test gas ($T=293$ K, $p=770$ mbar) while cell A was at vacuum. The measured spectrum under varying temperature condition is shown in ‘Circle’, the test gas temperatures in cell A and B were different, but the concentration and pressure were the same. These spectra and fitting residuals were used to derive an estimate on the optical sensitivity of the spectrometer on short time scales of seconds. The residual can be quantified by the statistical standard deviation of the residual over the spectral range, 1σ equals the OD noise. The peak values on the optical density ($OD = -\ln(I/I_0)$) scale and the 1σ of residuals were compared as the signal-to-noise ratio (SNR). The SNR result

is 312 for the circle curve in Fig. 6b. Dividing the concentration measured by the SNR, the noise equivalent concentration (NEC) or sensitivity is 32 ppm. It is also common to normalize the noise equivalent absorption coefficient with respect to the path length and the square root of the temporal bandwidth, which yields in this case $1.12 \times 10^{-4} \text{ cm}^{-1} \text{ Hz}^{-1/2}$. Note that all the spectra including those under conditions with temperature gradients presented in this paper were fitted with Voigt profile. The Voigt fitting for the measured spectra worked well for all the experimental conditions, there was no significant increase in the residuals comparing to the fitting in uniform condition.

The precision and stability of the sensor were investigated by means of the Allan deviation as shown in Fig. 6d, which was recorded for a stable CO_2 concentration 0.01 mol/mol. The Allan deviation plot follows the general behavior, first the precision is improved with the integration time while white noise is reduced, then for the longer time periods the precision gets limited by the long-term instabilities like thermal drifts. At 1 s averaging time, a precision of 7.3 ppm can be achieved. The Allan deviation plot indicates that the precision can be further improved to 1.7 ppm at 30 s of integration time.

Deviation of concentration measurements

To investigate the concentration measurement with LOS TDLAS technique under conditions with temperature gradients, cell A (T_2, L_2) was heated up to different temperatures from 293 to 430 K. In the experiments, only the temperature gradient was introduced, while the pressure and CO_2 concentration in both cells were kept constantly the same. In this demonstration, the p_i and $C_i (=C_{ave})$ shown in Fig. 2b were the same for each subsection. The measured deviation Δx was calculated by comparing the measured concentration x and the input test gas concentration C_{ave} , which can be known by measuring under uniform condition or from the test gas supplier. Figure 7 shows the measured and simulated concentrations (a) and deviations (b) under different temperature gradients. For all measurements, test gas temperature in cell B (T_1, L_1) was kept around room temperature (293 K), the pressure in both cells were 770 mbar. At each temperature point as shown by the x-axis in Fig. 7 (test gas temperature in cell A), the path-integrated spectral area was fitted, then the concentration was obtained using Eqs. 2 and 5 with different calculation temperatures (T_{ave}, T_{min} and T_{max}). The dotted and dashed lines in Fig. 7 show the measured results. The discrepancy between the derived concentrations with different calculation temperature increases as the temperature gradient increases. Also, the deviations increase as the temperature gradient increases for all curves. For clarity, only one error bar is shown for the first data point in Fig. 7a. The relative uncertainty of the concentration measurement was about 2% ($k=2$), that's the reason why the measured results are scattered. With the simulation method discussed in section 2, the deviations (concentrations) were simulated for each condition with different calculation temperature as shown in Fig. 7 (solid lines). The measured concentrations from path-integrated spectra and deviations are in good agreement with the simulation results. This verifies the proposed simulation methodology in section 2.

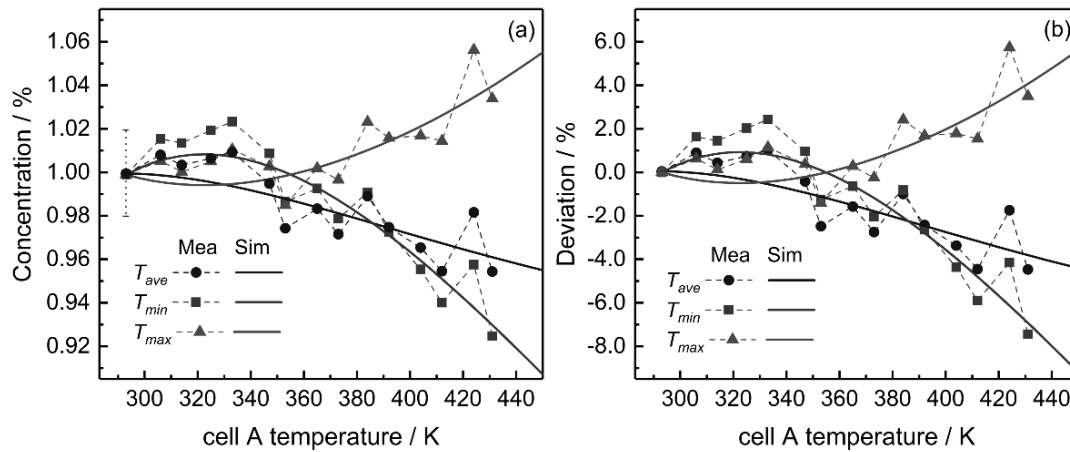


Figure 7. (a) Comparison of the measured and simulated concentration with different calculation temperatures. (b) The corresponding deviations.

Collisional width under conditions with temperature gradient

By holding the Doppler width fixed at the calculated value during Voigt fitting of the path-integrated spectrum, the collisional width (full width half maximum, FWHM) is extracted from the overall width of the absorption profile. The temperature dependence is determined by performing a power function fit of the measured collisional widths at various temperatures as shown in Fig. 8a. Note that the first and second terms on the right side of Eq. 4 are combined, one temperature dependence, n_{all} , was fitted. The spectra analyzed here were same as those used in Fig. 7, and the Doppler widths were calculated based on the path-averaged temperature T_{ave} . The collisional widths were extracted from the spectra under both constant (Square) and varying (Circle) conditions. The measured widths under uniform conditions show good agreement with an exponential fit as described by Eq. 5 leading to a value of $R^2 = 0.993$. The measured n_{all} is 0.77 ± 0.02 for the CO_2 P36e line in N_2 gas matrix (HITRAN2012 database $n_{air} = 0.76$). While, the measured n_{all} based on the collisional widths extracted from varying temperature conditions is incorrect. The larger the temperature gradient, the larger the discrepancy between the collisional widths of uniform and non-uniform conditions is observed.

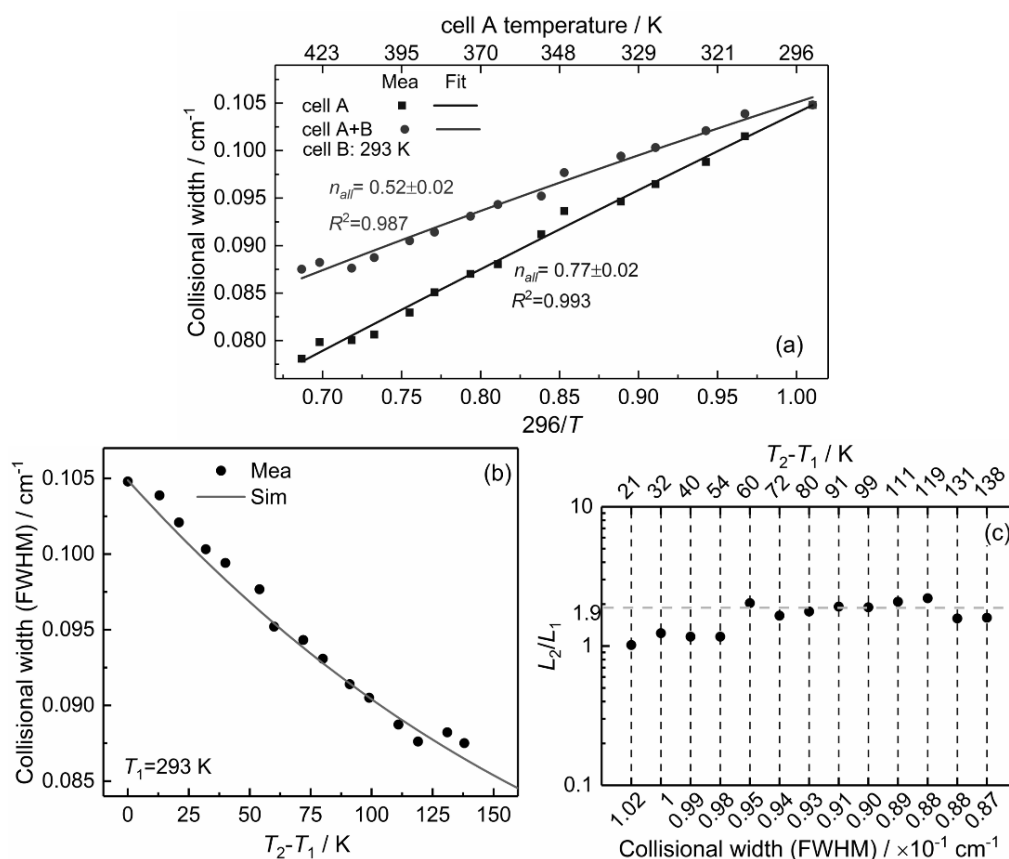


Figure 8. (a) Measured temperature dependence of the collisional width under uniform (Square) and non-uniform (Circle) conditions, and the nonlinear fits. (b) Comparison of measured and simulated collisional width under varying temperature conditions. (c) The calculated thermal boundary layer ratios using the measured collisional width based on Fig. 5b.

The measured collisional widths were compared with the simulated values from Fig. 5b, as shown in Fig. 8b. The measured results are in excellent agreement with the simulated collisional widths under the conditions with different thermal boundary layers. As discussed in section 2.5, the thermal boundary layer thickness can be estimated when knowing the collisional width, T_1 and T_2 . First, the relation between the collisional width and the ratio of L_2/L_1 for certain T_1 and T_2 temperatures should be simulated as shown in Fig. 5a. Then, the L_2/L_1 ratio can be derived by addressing the measured collisional width value on the simulated relationship curve. The estimated L_2/L_1 ratios were shown in Fig. 8c for different temperature gradients, the horizontal line indicates the real cell length ratio $L_2/L_1 = 1.9$ in the experiment. For large temperature gradients, the estimated L_2/L_1 ratios are closer to the true value. While simulating the relation between the collisional width and the ratio of L_2/L_1 , an initial gas concentration is needed. For the gas species with very low concentration (e.g. <1%), the first term on the right side of Eq. 4 is rather small comparing with the second term. The initial gas concentration in the simulation is not crucial for using the collisional width to estimate the thermal boundary layer information. But if the target gas has high concentration i.e. >10~20%, it is necessary to have the knowledge of the concentration when doing the simulation.

Conclusion

We have developed a new methodology for quantifying the thermal boundary layer effects on LOS TDLAS measurements. A dTDLAS spectrometer with two gas cells was implemented to achieve the temperature gradients along the LOS and validate the simulation results. The spectrometer was applied to the detection of CO₂ concentrations and collisional widths under

uniform and non-uniform conditions using different calculation temperatures (T_{ave} , T_{min} or T_{max}). Open-path TDLAS instruments, despite being widely used, have so far rarely been investigated for LOS gradients effects on concentration measurements, although they may be small. To our knowledge, the quantification of the effects of thermal boundary layers on LOS TDLAS based concentration and collisional width measurements has been presented for the first time. The simulated deviations, collisional widths and estimated boundary layer thickness show very good agreement with the experimental results. This method will facilitate further investigation of the performance (e.g. systematic deviations) of commercial TDLAS instruments used in conditions with temperature gradients. Additionally, this simulation method can also be used to evaluate whether the transition line is suitable for certain non-uniform conditions with allowable deviation. Further measurements and simulations will be performed to extend the method to concentration and/or pressure gradients.

Conflict of Interest

The authors report there are no conflicts of interest.

Funding

This work was supported by the IMPRESS project within the European Metrology Research Programme (EMRP). The EMRP is jointly funded by the EMRP participating countries within EURAMET and the European Union.

Reference

1. V. Ebert, J. Wolfrum. "Absorption Spectroscopy". In: F. Mayinger, O. Feldmann, editors. Optical Measurements—Techniques and Applications, 2nd corr. edition. (Heat and Mass Transfer), Heidelberg, München: Springer Verlag, 2001. 227-265.
2. J. A. Nwaboh, Z. Qu, O. Werhahn, V. Ebert. "Interband cascade laser-based optical transfer standard for atmospheric carbon monoxide measurements". Appl. Opt. 2017. 56(11): E84-E93.
3. Z. Qu, E. Steinvall, R. Ghorbani, F. M. Schmidt. "Tunable Diode Laser Atomic Absorption Spectroscopy for Detection of Potassium under Optically Thick Conditions". Anal. Chem. 2016. 88 (7): 3754-60.
4. C. S. Goldenstein, R. M. Spearrin, J. B. Jeffries, R. K. Hanson. "Infrared laser-absorption sensing for combustion gases". Prog. Energy Combust. Sci. 2017. 60: 132-176.
5. R. K. Hanson. "Applications of quantitative laser sensors to kinetics, propulsion and practical energy systems". Proc. Combust. Inst. 2011. 33(1): 1-40.

6. X. Ouyang, P. L. Varghese. "Line-of-sight absorption measurements of high temperature gases with thermal and concentration boundary layers". *Appl. Opt.* 1989. 28(18): 3979-3984.
7. S. Ciężczyk. "A Local Model and Calibration Set Ensemble Strategy for Open-Path FTIR Gas Measurement with Varying Temperature". *Metrol. Meas. Syst.* 2013. 20(3): 513-524.
8. Z. Qu, R. Ghorbani, D. Valiev, F. M. Schmidt. "Calibration-free scanned wavelength modulation spectroscopy--application to H₂O and temperature sensing in flames". *Opt. Express* 2015. 23 (12): 16492-16499.
9. S. Wagner, B. T. Fisher, J. W. Fleming, V. Ebert. "TDLAS-based in situ measurement of absolute acetylene concentrations in laminar 2D diffusion flames". *Proc. Combust. Inst.* 2009. 32 (1): 839-846.
10. J. Wang, M. Maiorov, J. B. Jeffries, D. Z. Garbuzov, J. C. Connolly, R. K. Hanson. "A potential remote sensor of CO in vehicle exhausts using 2.3 μ m diode lasers". *Meas. Sci. Technol.* 2000. 11 (11): 1576.
11. A. Sepman, Y. Ögren, Z. Qu, H. Wiinikka, F. M., Schmidt. "Real-time in situ multi-parameter TDLAS sensing in the reactor core of an entrained-flow biomass gasifier". *Proc. Combust. Inst.* 2017. 36 (3): 4541-4548.
12. S. Wagner, M. Klein, T. Kathrotia, U. Riedel, T. Kissel, A. Dreizler, V. Ebert. "Absolute, spatially resolved, in situ CO profiles in atmospheric laminar counter-flow diffusion flames using 2.3 μ m TDLAS". *Appl. Phys. B: Lasers Opt.* 2012. 109 (3): 533-540.
13. J. Girard, R. Spearrin, C. Goldenstein, R. K. Hanson. "Compact optical probe for flame temperature and carbon dioxide using interband cascade laser absorption near 4.2 μ m". *Combust. Flame* 2017. 178: 158-167.
14. K. Sun, R. Sur,; X. Chao, J. B. Jeffries, R. K. Hanson, R. J. Pummill, K. J. Whitty. "TDL absorption sensors for gas temperature and concentrations in a high-pressure entrained-flow coal gasifier". *Proc. Combust. Inst.* 2013. 34 (2): 3593-3601.

15. C. S. Goldenstein, C. A. Almodóvar, J. B. Jeffries, R. K. Hanson, C. M. Brophy. “High-bandwidth scanned-wavelength-modulation spectroscopy sensors for temperature and H₂O in a rotating detonation engine”. *Meas. Sci. Technol.* 2014. 25 (10): 105104.
16. C. S. Goldenstein, I. A. Schultz, J. B. Jeffries, R. K. Hanson. “Two-color absorption spectroscopy strategy for measuring the column density and path average temperature of the absorbing species in nonuniform gases”. *Appl. Opt.* 2013. 52 (33): 7950-62.
17. F. Li, X. Yu, W. Cai, L. Ma. “Uncertainty in velocity measurement based on diode-laser absorption in nonuniform flows”. *Appl. Opt.* 2012. 51 (20): 4788-4797.
18. L. S. Chang, C. L. Strand, Jeffries, J. B. Jeffries, R. K. Hanson. G. S. Diskin, R. L. Gaffney, D. P. Capriotti. “Supersonic Mass-Flux Measurements via Tunable Diode Laser Absorption and Nonuniform Flow Modeling”. *AIAA J.* 2011. 49 (12): 2783-2791.
19. M. Schoenung, R. K. Hanson. “CO and Temperature Measurements in a Flat Flame by Laser Absorption Spectroscopy and Probe Techniques”. *Combust. Sci. Technol.* 1980. 24 (5-6): 227-237.
20. W. Cai, C. F. Kaminski. “Tomographic absorption spectroscopy for the study of gas dynamics and reactive flows”. *Prog. Energy Combust. Sci.* 2017. 59: 1-31.
21. X. Liu, J. B. Jeffries, R. K. Hanson. “Measurement of Non-Uniform Temperature Distributions Using Line-of-Sight Absorption Spectroscopy”. *AIAA J.* 2007. 45 (2): 411-419.
22. S. T. Sanders, J. Wang, J. B. Jeffries, R. K. Hanson. “Diode-laser absorption sensor for line-of-sight gas temperature distributions”. *Appl. Opt.* 2001. 40 (24): 4404-4415.
23. C. Liu; L. Xu, Z. Cao. “Measurement of nonuniform temperature and concentration distributions by combining line-of-sight tunable diode laser absorption spectroscopy with regularization methods”. *Appl. Opt.* 2013. 52 (20): 4827-4842.
24. A. Seidel, S. Wagner, A. Dreizler, V. Ebert. “Robust, spatially scanning, open-path TDLAS hygrometer using retro-reflective foils for fast tomographic 2-D water vapor concentration field measurements”. *Atmos. Meas. Tech.* 2015. 8 (5): 2061-2068.

25. A. Pogány, S. Wagner, O. Werhahn, V. Ebert. “Development and metrological characterization of a tunable diode laser absorption spectroscopy (TDLAS) spectrometer for simultaneous absolute measurement of carbon dioxide and water vapor”. Appl. Spectrosc. 2015. 69 (2): 257-268.
26. N. Lüttschwager, A. Pogány, J. Nwaboh, A. Klein, B. Buchholz, O. Werhahn, V. Ebert. “In Traceable amount of substance fraction measurements in gases through infrared spectroscopy at PTB”. 17th International Congress of Metrology 2015. EDP Sciences: 07005.
27. L.S. Rothman, I.E. Gordon, Y. Babikov, A. Barbe, D. Chris Benner, P.F. Bernath, M. Birk, L. Bizzocchi, V. Boudon, L.R. Brown, A. Campargue, K. Chance, E.A. Cohen, L.H. Coudert, V.M. Devi, B.J. Drouin, A. Fayt, J.-M. Flaud, R.R. Gamache, J.J. Harrison, J.-M. Hartmann, C. Hill, J.T. Hodges, D. Jacquemart, A. Jolly, J. Lamouroux, R.J. Roy Le, G. Li, D.A. Long, O.M. Lyulin, C.J. Mackie, S.T. Massie, S. Mikhailenko, H.S.P. Müller, O.V. Naumenko, A.V. Nikitin, J. Orphal, V. Perevalov, A. Perrin, E.R. Polovtseva, C. Richard, M.A.H. Smith, E. Starikova, K. Sung, S. Tashkun, J. Tennyson, G.C. Toon, V.G. Tyuterev, J. Vander Auwera, G. Wagner. “The HITRAN2012 Molecular Spectroscopic Database”. J. Quant. Spectrosc. Radiat. Transfer 2013. 130: 4-50.
28. A. Pogány, O. Ott, O. Werhahn, V. Ebert. “Towards traceability in CO₂ line strength measurements by TDLAS at 2.7 μ m”. J. Quant. Spectrosc. Radiat. Transfer 2013. 130: 147-157.